Extended isogeometric boundary element method (XIBEM) for two-dimensional Helmholtz problems

M.J. Peake*, J. Trevelyan, G. Coates

Durham University, School of Engineering and Computing Sciences, Durham, DH1 3LE, United Kingdom

Abstract

Isogeometric analysis is a topic of considerable interest in the field of numerical analysis. The boundary element method (BEM) requires only the bounding surface of geometries to be described; this makes non-uniform rational B-splines (NURBS), which commonly describe the bounding curve or surface of geometries in CAD software, appear to be a natural tool for the approach. This isogeometric analysis BEM (IGABEM) provides accuracy benefits over conventional BEM schemes due to the analytical geometry provided by NURBS. When applied to wave problems, it has been shown that enriching BEM approximations with a partition-of-unity basis, in what has become known as the PU-BEM, allows highly accurate solutions to be obtained with a much reduced number of degrees of freedom. This paper combines these approaches and presents an extended isogeometric BEM (XIBEM) which uses partition-of-unity enriched NURBS functions; this new approach provides benefits which surpass those of both the IGABEM and the PU-BEM. Two

*Corresponding author

Email address: m.j.peake@durham.ac.uk (M.J. Peake)

Preprint submitted to Computer Method in Applied Mechanics and EngineeringMarch 22, 2013

numerical examples are given: a single scattering cylinder and a multiple-scatterer made up of two capsules and a cylinder.
Keywords: Helmholtz, acoustics, isogeometric analysis, boundary element method, partition of unity

---

1. Introduction

Creating a suitable mesh can be a significantly complicated and time-consuming stage in numerical analysis. Techniques that improve mesh quality or reduce the time required to make a suitable mesh are of interest to both the academic and industrial communities. To this end, Hughes *et al.* [1] presented isogeometric analysis (IGA): the concept of using the basis functions that describe a geometry in computer-aided design (CAD) to construct exact geometries for numerical analysis. Most numerical analysis software makes use of Lagrangian shape functions to describe the geometry and unknown fields of a problem; Hughes *et al.* showed that using non-uniform rational B-splines (NURBS) as the basis for analysis provided accuracy benefits over the former approach. IGA also greatly reduces the difficulties of creating and refining a mesh; this is apparent particularly for large, complex geometries. Most isogeometric analysis papers have considered the use of NURBS; however, more recently, other basis functions have been investigated such as T-splines [2].

[1] and much of the early research in the isogeometric field applied IGA in the context of the finite element method (FEM). Applications include structural vibrations [3], fluid-structure interaction [4] and electromagnetics [5]. Isogeometric analysis has also been coupled with existing enriched FEM ap-

proaches such as XFEM; De Luycker *et al.* [6] presented such a combination for problems in fracture mechanics.

The work presented in this paper focuses on the use of the boundary element method (BEM). The BEM provides benefits over the FEM for some classes of problems, such as the acoustic wave scattering in infinite domains considered here. Unlike the FEM, the BEM requires only the boundary of scattering objects to be meshed. There is no truncation of infinite domains and no artificial boundary conditions are used to model infinity; the formulation of the boundary integral equation (BIE) inherently deals with such domains.

NURBS, ubiquitous in CAD software, also only describe the boundary of the geometries being modelled; hence, IGA and BEM would appear to be a natural combination. Indeed, the benefit of using the NURBS surface definition directly to find analytical geometry functions is more apparent for BEM simulations that for the FEM. NURBS solids do exist and this is the basis of isogeometric FEM. However, given that CAD systems generally only use a boundary representation of solids, isogeometric FEM requires a preprocessing stage to create such a solid from the NURBS-based boundary. This is a complex process in comparison to a boundary-only approach. Some research has already been conducted in the field of isogeometric boundary element methods: Simpson *et al.* [7] applied the approach to elastostatic analysis, coining the term IGABEM; Politis *et al.* [8] considered problems of potential flow; Takahashi and Matsumoto [9] applied the fast multipole method to IGABEM for the Laplace equation; and Scott *et al.* [10] employed T-splines for elastostatic problems.

Like the FEM, conventional BEM schemes require a mesh to be refined as the wavenumber, k, of a problem increases. This imposes a practical limit, given a fixed computational resource, on the wavenumber that can be considered for a specific problem geometry. A number of approaches have been developed in an attempt to increase this limit.

Abboud *et al.* [11] showed that, for convex scatterers of size $\gg \lambda$ (the wavelength), the scattered potential may be approximated as the product of a slowly varying function and the incident wave. Bruno *et al.* [12] presented an approach with complexity independent of wavelength by restricting the interval over which boundary integrals are performed to small regions in the immediate vicinity of stationary points; Langdon and Chandler-Wilde [13] have shown that this approach is suitable for polygonal scatterers; Domínguez *et al.* [14] demonstrated that, for problems of asymptotically large wavenumbers, the required number of degrees of freedom increases only with $\mathcal{O}(k^{1/9})$, for a fixed error bound; Anand *et al.* [15] extended this approach for problems of multiple scatterers.

In this paper, the partition of unity method (PUM), developed by Melenk and Babuška [16], is used. The idea behind the PUM, in which a basis comprising multiple plane waves is used as the approximating function, was previously used with the BEM for acoustic wave scattering by de la Bourdonnaye [17] under the name 'microlocal discretization'; Bériot *et al.* [18] applied the approach to the Galerkin BEM and Perrey-Debain *et al.* [19] applied it to the collocation BEM. Perrey-Debain *et al.* compared a conventional BEM with a partition of unity BEM (PU-BEM) for a two-dimensional wave scattering problem; they demonstrated that the number of degrees of

freedom required, to achieve the same accuracy, could be reduced from ten degrees of freedom per wavelength (conventional BEM) to, just over, two per wavelength (PU-BEM).

This paper introduces a new isogeometric, collocation BEM employing the PUM; the approach is named the eXtended Isogeometric BEM (XIBEM). The scheme is developed for two-dimensional acoustic wave scattering problems and it is shown that this advancement on IGABEM improves the accuracy of simulations and, with the same computational resource, extends simulations to higher frequencies.

2. NURBS

The basis of the method presented in this paper, and in many other isogeometric analysis papers, includes NURBS; therefore, an understanding of such splines is important. An in-depth discussion of the topic can be found in [20]. Here, a short overview of the topic is presented to demonstrate some of the terminology and nomenclature later used.

Splines are most typically used to model geometric curves and surfaces; however, splines can be used to represent any kind of numerical data such as temperature or velocity. Data points, geometrical coordinates or otherwise, are referred to as *control points*, $\mathbf{P}_j$; each control point has an associated NURBS *basis function*[1]. In this regard, NURBS are similar to the conventional Lagrangian approximations, with nodes and shape functions, used in many finite element and boundary element analyses; they also provide a par-

[1]Control points are not necessarily interpolation points. In geometrical representations, many of the control points lie off the surface being modelled.

tition of unity which is an important property for the enrichment method presented in this paper.

A defining feature of a NURBS curve is the *knot vector* Ξ. This is a sequence of real numbers, referred to as knots ξ_j. There are $s+1$ knots in Ξ and they are non-decreasing; thus, $\xi_j \leq \xi_{j+1}$ for $j = 0, \ldots, s-1$. In the current work, it is assumed that a knot vector takes the form

$$\Xi = \{\underbrace{0, \ldots, 0}_{p+1}, \xi_{p+1}, \ldots, \xi_{s-p+1}, \underbrace{1, \ldots, 1}_{p+1}\}. \tag{1}$$

The jth B-spline basis function of pth-degree is denoted by $N_{j,p}(\xi)$. For $p = 0$, it is defined as

$$N_{j,0}(\xi) = \begin{cases} 1 & \text{if } \xi_j \leq \xi < \xi_{j+1} \\ 0 & \text{otherwise,} \end{cases} \tag{2}$$

and, for $p = 1, 2, 3, \ldots$,

$$N_{j,p}(\xi) = \frac{\xi - \xi_j}{\xi_{j+p} - \xi_j} N_{j,p-1}(\xi) + \frac{\xi_{j+p+1} - \xi}{\xi_{j+p+1} - \xi_{j+1}} N_{j+1,p-1}(\xi). \tag{3}$$

There are $J+1$ B-spline basis functions and $J = s - p - 1$.

With a NURBS curve, each control point, and thus B-spline basis function, has a weighting, $w_j > 0$; B-splines can be considered a special case of NURBS in which all w_j have the same value. A pth-degree NURBS representation is defined by

$$\mathbf{F}(\xi) = \frac{\sum_{j=0}^{J} N_{j,p}(\xi) w_j \mathbf{P}_j}{\sum_{j=0}^{J} N_{j,p}(\xi) w_j}, \qquad 0 \leq \xi \leq 1. \tag{4}$$

If it is assumed that

$$R_{j,p}(\xi) = \frac{N_{j,p}(\xi) w_j}{\sum_{i=0}^{J} N_{i,p}(\xi) w_i}, \tag{5}$$

(4) can be rewritten in the form

$$\mathbf{F}(\xi) = \sum_{j=0}^{J} R_{j,p}(\xi) \mathbf{P}_j. \tag{6}$$

Applying a weighting to each of the B-spline basis functions allows more complex geometries to be modelled. A specific example is the circular arc: a quarter of a circular arc cannot be expressed analytically using a Lagrangian or B-spline interpolation; however, NURBS can model the curve exactly using three control points and appropriate weights.

3. Formulation of XIBEM for the Helmholtz equation

3.1. Boundary integral equation

Let $\Omega \subset \mathbb{R}^2$ be an infinite acoustic domain containing a smooth scatterer of boundary $\Gamma := \partial\Omega$. Assuming a time dependence, $\exp(-i\omega t)$, the wave equation is reduced to the well-known Helmholtz equation:

$$\Delta\phi(\mathbf{q}) + k^2\phi(\mathbf{q}) = 0, \quad \phi \in \mathbb{C}, \mathbf{q} \in \Omega, \tag{7}$$

where $\Delta(\cdot)$ is the Laplacian operator, $\phi(\mathbf{q})$ is the wave potential at point $\mathbf{q}$, and $k = 2\pi/\lambda$ is the wavenumber. For scattering problems, an exterior wave is required; here, the scatterer is impinged by an incident plane wave,

$$\phi^{\mathrm{I}}(\mathbf{q}) = A^{\mathrm{I}} \exp\left(ik\mathbf{d}^{\mathrm{I}} \cdot \mathbf{q}\right), \quad \left|\mathbf{d}^{\mathrm{I}}\right| = 1, \tag{8}$$

where $A^{\mathrm{I}} \in \mathbb{C}$ is the plane wave amplitude and the unit-vector, $\mathbf{d}^{\mathrm{I}}$, is its direction of propagation.

The process of obtaining the BIE using Green's second identity and (7) is well-known [21]. It yields

$$c(\mathbf{p})\phi(\mathbf{p}) = \int_\Gamma \left[\frac{\partial \phi(\mathbf{q})}{\partial n} G(\mathbf{p},\mathbf{q}) - \phi(\mathbf{q}) \frac{\partial G(\mathbf{p},\mathbf{q})}{\partial n} \right] \mathrm{d}\Gamma(\mathbf{q}) + \phi^{\mathrm{I}}(\mathbf{p}), \quad \mathbf{p},\mathbf{q} \in \Gamma, \tag{9}$$

where n is the outward-pointing normal at the integration point $\mathbf{q}$ and, assuming Γ is smooth, $c(\mathbf{p}) = 1/2$ at the evaluation point $\mathbf{p}$. Further, $G(\mathbf{p},\mathbf{q})$ is the Green's function, representing the field effect experienced at $\mathbf{q}$ due to a unit source at $\mathbf{p}$ (or *vice versa*); in two-dimensional space, it is

$$G(\mathbf{p},\mathbf{q}) = \frac{i}{4} H_0^{(1)}(kr), \tag{10}$$

where $H_0^{(1)}(\cdot)$ is a Hankel function of the first kind, order zero, and $r = |\mathbf{p}-\mathbf{q}|$.

A solution to (7) is sought, subject to a general Robin boundary condition,

$$\frac{\partial \phi(\mathbf{q})}{\partial n} = \beta(\mathbf{q})\phi(\mathbf{q}) + \gamma(\mathbf{q}), \tag{11}$$

thus (9) is reformulated as

$$c(\mathbf{p})\phi(\mathbf{p}) + \int_\Gamma \left[\frac{\partial G(\mathbf{p},\mathbf{q})}{\partial n} - G(\mathbf{p},\mathbf{q})\beta(\mathbf{q}) \right] \phi(\mathbf{q})\, \mathrm{d}\Gamma(\mathbf{q}) = \int_\Gamma G(\mathbf{p},\mathbf{q})\gamma(\mathbf{q})\, \mathrm{d}\Gamma(\mathbf{q}) + \phi^{\mathrm{I}}(\mathbf{p}). \tag{12}$$

$\gamma(\mathbf{q})$ is non-zero for active boundary conditions (radiation problems) and zero for passive boundary conditions; $\beta(\mathbf{q})$ is an impedance property of the scatterer. For compact presentation, only one boundary condition is considered: the case of a perfectly reflecting ("sound-hard") cylinder where

$\beta(\mathbf{q}) = \gamma(\mathbf{q}) = 0$. (12) is now reformulated as

$$c(\mathbf{p})\phi(\mathbf{p}) + \int_\Gamma \frac{\partial G(\mathbf{p},\mathbf{q})}{\partial n}\phi(\mathbf{q})\,\mathrm{d}\Gamma(\mathbf{q}) = \phi^{\mathrm{I}}(\mathbf{p}). \tag{13}$$

3.2. IGABEM

In the classical, collocation BEM, Γ is now discretised into elements on which the geometry and ϕ are approximated with polynomial, isoparametric elements [22]. Here, instead of piecewise polynomial elements, it is assumed that the scatterer can be expressed as a NURBS expansion.

The relationship described in (6) provides an analytical geometry given by the mapping

$$\Gamma = \{\mathbf{F}(\xi) : \xi \in [0,1)\}, \tag{14}$$

where $\mathbf{F} : \mathbb{R} \to \mathbb{R}^2$. This mapping between $\mathbf{q} \in \Gamma$ and ξ is unique and, hence, it is assumed that any function $f(\mathbf{q})$ is equivalent to $f(\xi)$. The variation of potential over Γ can now be formally expressed in terms of a NURBS expression,

$$\phi(\xi) = \sum_{j=0}^{J} R_{j,p}(\xi)\phi_j, \tag{15}$$

where ϕ_j are unknown "control" potentials associated with each NURBS basis function, $R_{j,p}$. Substitution of (15) into (13) gives the IGABEM boundary integral equation,

$$c(\mathbf{p})\phi(\mathbf{p}) + \sum_{j=0}^{J}\int_0^1 \frac{\partial G(\mathbf{p},\mathbf{q})}{\partial n} R_{j,p}(\xi)|J_\xi|\,\mathrm{d}\xi\,\phi_j = \phi^{\mathrm{I}}(\mathbf{p}), \tag{16}$$

where $|J_\xi|$ is the Jacobian of the mapping in (14).

To find the unknown potentials on Γ, (16) is collocated at a sufficient number of points on the boundary to yield a system of linear equations

that can be solved in a conventional fashion. The integrals within (16) can be evaluated with appropriate quadrature; the BEM literature has a rich variety of discussion on this subject including [23, 24]. In the conventional BEM, collocation points are placed on nodal points. This is not possible in IGABEM because geometry control points can lie off the boundary. Instead, the Greville abscissae [25, 26] are used, denoted by $\hat{\xi}_g$ and calculated using the NURBS knot vector:

$$\hat{\xi}_g = \frac{\xi_{g+1} + \xi_{g+2} + \cdots + \xi_{g+p-1}}{p}, \quad g = 1, 2, \ldots, J. \tag{17}$$

Although there are $J+1$ NURBS functions and control points, the Greville abscissae provide only J collocation points. However, the first and last control points of a boundary will be equal; thus, the first and last NURBS basis functions are combined and the control points are considered to be one. This is similar to the conventional BEM approach.

3.3. XIBEM

The extended IGABEM introduces a linear, partition-of-unity expansion of plane waves on each NURBS basis function so that (15) is reformulated,

$$\phi(\xi) = \sum_{j=0}^{J} R_{j,p}(\xi) \sum_{m=0}^{M} A_{jm} \exp\left(ik\mathbf{d}_{jm} \cdot \mathbf{q}(\xi)\right), \quad |\mathbf{d}_{jm}| = 1, \tag{18}$$

where there are $M+1$ plane waves in each expansion with prescribed directions of propagation, $\mathbf{d}_{jm} \in \mathbb{R}^2$, and unknown amplitudes, $A_{jm} \in \mathbb{C}$.

The substitution of (18) into (13) yields

$$c(\mathbf{p})\phi(\mathbf{p}) + \sum_{j=0}^{J} \sum_{m=0}^{M} h_{jm}\, A_{jm} = \phi^{\mathrm{I}}(\mathbf{p}), \tag{19}$$

where

$$h_{jm} = \int_0^1 \frac{\partial G(\mathbf{p}, \mathbf{q})}{\partial n} R_{j,p}(\xi) \exp\left(ik\, \mathbf{d}_{jm} \cdot \mathbf{q}(\xi)\right) |J_\xi| \, \mathrm{d}\xi. \tag{20}$$

This is the discretised form of the BIE for XIBEM which can be collocated in order to solve (7).

In order to introduce a convenient measure of computational efficiency, the parameter, τ, is defined as the number of degrees of freedom per wavelength on Γ. More explicitly, the total number of degrees of freedom JM is equal to τ multiplied by the number of wavelengths needed to describe Λ. To obtain the desired τ, one is free to increase J through knot refinement and/or M by including more plane waves in each basis. For multiple scatterers of different sizes, M can be set globally or locally. It has been found that keeping elements or knot spans similar in length and using a global value of M provides better conditioning than varying M; however, good solutions can be obtained using either approach. In the PU-BEM, it has been found that increasing M and using fewer elements provides a greater accuracy; however, this has not been explored in XIBEM and is a topic of future research. For an accuracy $\sim 1\%$, a heuristic rule states that finite element and boundary element approximations generally require $\tau \geq 10$; however, it will be shown that, for XIBEM, this requirement is significantly reduced. In this paper, the plane wave directions are defined to be equally distributed around the unit circle:

$$\mathbf{d}_{jm} = \left(\cos\theta_{jm}, \sin\theta_{jm}\right), \quad \theta_{jm} = \frac{2m\pi}{M+1} + \theta^{\mathrm{I}}, \tag{21}$$

where θ^{I} is the angle of incidence of the incident plane wave; this guarantees the inclusion of the incident wave direction in the basis. This direction is included because, for asymptotically large k, the potential in the illuminated

zone takes a value of $2\phi^{\mathrm{I}}$. It should be noted that θ^{I} does not have to be included in $\mathbf{d}_{jm}$ and highly accurate results are still obtained if it is omitted. For problems of multiple incident waves, each incident wave could be included in the basis; however, if incident angles are very similar, this could lead to poor conditioning of the system matrices.

The inclusion of multiple plane waves – and thus degrees of freedom – on each NURBS basis function means that collocation at nodal points or the Greville abscissae no longer provides a sufficient number of collocation points. To find the potential on Γ, (19) is collocated at a set of $Z = (J+1)(M+1)$ collocation points, $\mathbf{p}_z$, where $z = 0, \ldots, Z-1$. This points are equally-spaced on the local coordinate, $\xi \in [0, 1)$. Z is equal to the total number of unknown amplitudes, A_{jm}, that are sought. This yields a square system of linear equations,

$$[\mathbf{C} + \mathbf{H}]\{\mathbf{x}\} = \{\mathbf{b}\}, \tag{22}$$

where the (usually sparse) square matrix $[\mathbf{C}]$ results from interpolations of the plane waves at $\mathbf{p}$ using (18) to write the first term in (19); the right-hand side vector $\{\mathbf{b}\}$ contains the incident wave potentials at the collocation points; and the unknown vector $\{\mathbf{x}\}$ contains the unknown amplitudes, A_{jm}. Further, the square matrix $[\mathbf{H}]$ is fully populated with integrals from (20).

It should be recalled that for wave problems the Greens function is oscillatory and that all integrations need to be evaluated using a sufficient number of points to capture that oscillation, even in the far field. This is true for conventional BEM as well as plane wave enriched BEM. Thus, the fact that plane wave enriched BEM approximations involve elements that can span many wavelengths does not in itself increase the total number of integration

points required to assemble the system of equations. However, the inclusion of the plane wave enrichment does have some implications on the required number of integration points, in that it changes the apparent wavelength of the oscillatory integrand to $\bar{\lambda}$, where $\bar{\lambda} \in (0, 2\lambda)$. For this reason, although some authors have presented novel integration schemes that offer promise for rapid evaluation of these boundary integrals [27, 28, 29], in the current work, which is aimed at demonstrating the XIBEM formulation for the first time, we simply use an average integration point spacing of $\lambda/24$. This has the effect of increasing the time required for the matrix assembly somewhat, but the reduction in the size of the system means that plane wave enriched BEM significantly outperforms conventional, unenriched approximations.

4. Numerical results

The XIBEM can be used to solve wave scattering problems involving single or multiple scatterers. As in the derivation, a perfectly reflecting boundary condition is applied to all scatterers in the following examples. In the authors' implementation, the boundary is subdivided into cells of approximately $\lambda/4$ in length and the boundary integrals are evaluated cell by cell using sixth-order quadrature. The CHIEF method [30] is used to overcome the well-known nonuniqueness problem associated with solving the Helmholtz equation with the BEM. The authors use a truncated singular value decomposition (SVD) to solve the resulting system.

All errors, $\mathcal{E}$, are evaluated in a relative L_2-norm sense,

$$\mathcal{E} = \frac{\left\| \boldsymbol{\Phi} - \boldsymbol{\Phi}^{\mathrm{ref}} \right\|_{L_2(\Gamma)}}{\left\| \boldsymbol{\Phi}^{\mathrm{ref}} \right\|_{L_2(\Gamma)}}, \tag{23}$$

where $\mathbf{\Phi}$ is a vector containing potentials, at points along the boundary of the scatterer, evaluated by a numerical simulation; $\mathbf{\Phi}^{\text{ref}}$ is a vector of potentials calculated by analytical solution (if available) or by an appropriate converged reference solution. The potentials are calculated at 1000 equally spaced points around each boundary and so the norms can be calculated in a trapezoidal rule sense.

In this paper, four types of simulation are referred to: *conventional BEM* implies a piecewise, polynomial BEM using continuous, isoparametric, quadratic elements; *IGABEM* implies an isogeometric BEM using NURBS to describe the geometry and potential function of the scatterer; *XIBEM* refers to the extended IGABEM where the NURBS basis functions approximating the potential over the boundary are enriched with a linear combination of plane waves; *PU-BEM* refers to a partition-of-unity BEM such as in [19].

4.1. Unit cylinder

Consider a cylinder of radius $a = 1$, centred at the origin. The cylinder is impinged by an incident plane wave of amplitude $A^{\text{I}} = 1$, and which propagates in the direction $\mathbf{d}^{\text{I}} = (1, 0)$ – angle of incidence $\theta^{\text{I}} = 0$ radians. The total (incident and scattered) potential at a point, $\mathbf{q} \in \Omega$, can be calculated using the infinite series, adapted from [31],

$$\phi(\mathbf{q}) = \phi^{\text{I}}(\mathbf{q}) - \frac{J_0'(ka)}{H_0'(ka)} H_0(kr) - 2\sum_{n=1}^{\infty} i^n \frac{J_n'(ka)}{H_n'(ka)} H_n(kr)\cos(n\theta), \qquad (24)$$

where $\mathbf{q} = r(\cos\theta, \sin\theta)$, $J_n'(\cdot)$ denotes the derivative of the Bessel function of the first kind and order n, and $H_n'(\cdot)$ denotes the derivative of $H_n(\cdot)$. If $\mathbf{q}$

is on the surface of the scatterer, $r = a$ and (24) reduces to

$$\phi(\mathbf{q}) = \frac{2}{\pi ka}\left[\frac{i}{H_0'(ka)} + 2\sum_{n=1}^{\infty}\frac{i^{n+1}}{H_n'(ka)}\cos(n\theta)\right]. \tag{25}$$

The NURBS-based mesh of a cylinder in this paper consists of a square of nine control points, shown in Fig. 1, and NURBS basis functions, of degree $p = 2$, displayed in Fig. 2.

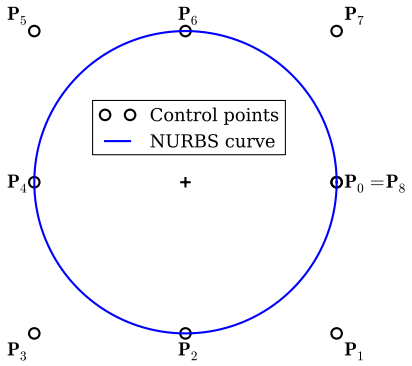

Figure 1: Unit-circle NURBS curve.

Initially, a comparison between the conventional BEM and the IGABEM is sought. The quality of the solution $\mathbf{\Phi}$ over a range of ka is investigated. As ka increases, the degrees of freedom are added to maintain that the number of degrees of freedom per wavelength of the problem, $\tau \approx 10$. In the conventional BEM, the number of elements E must increase as $\tau = 2E/ka$. This is simply achieved by defining E elements of uniform size describing the circumference of the circle. In the IGABEM case, $\tau = (J+1)/ka$, so more NURBS functions are required; a process of *knot refinement* [20] – inserting knots into the knot vector and creating new control points – is used to create these extra functions. In this work, the inserted knots are equally spaced,

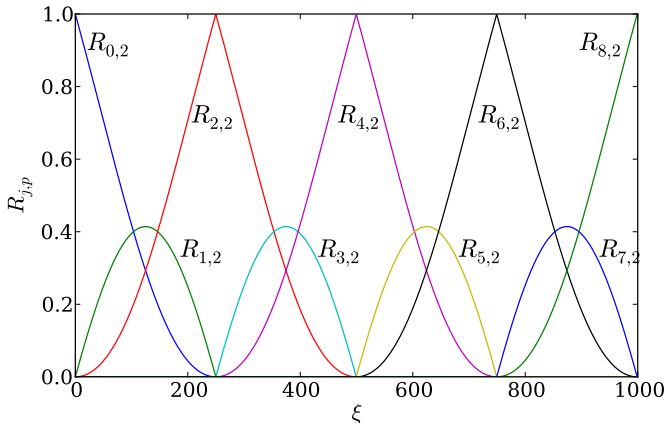

Figure 2: NURBS basis functions for unit-circle of degree $p = 2$, with knot vector $\Xi = \{0, 0, 0, 0.25, 0.25, 0.5, 0.5, 0.75, 0.75, 1, 1, 1\}$ and weighting $w_j = \{1, 1/\sqrt{2}, 1, 1/\sqrt{2}, 1, 1/\sqrt{2}, 1, 1/\sqrt{2}, 1\}$.

on the local coordinate, between existing knots. Due to the integer nature of the additions of degrees of freedom, τ cannot be guaranteed to be exactly 10 for all simulations.

The integrals in the conventional BEM are evaluated using six-point quadrature over each element. The integrals in the IGABEM are evaluated using six-point quadrature over each knot span, i.e. between each value of knot in the knot vector. Higher order integration quadrature has been tested; however, the authors found that the results using the scheme above were converged, so the results presented are due to the discretisation only.

Fig. 3 shows the errors, $\mathcal{E}$, of the simulations using these two methods. The integer nature of addition of elements or knots, to maintain $\tau \approx 10$, causes the sawtooth effect observed at lower values of ka. IGABEM clearly provides a greater accuracy of approximation with both meshes; this improvement in accuracy is approximately one order of magnitude for $ka > 10$. The greater accuracy is due to the integration points being mapped to the

analytical surface of the cylinder by the NURBS functions; the polynomial functions of the conventional BEM provide only an approximation to the geometry. These same functions approximate the wave potential over the boundary and so greater accuracy is also obtained here by the NURBS functions.

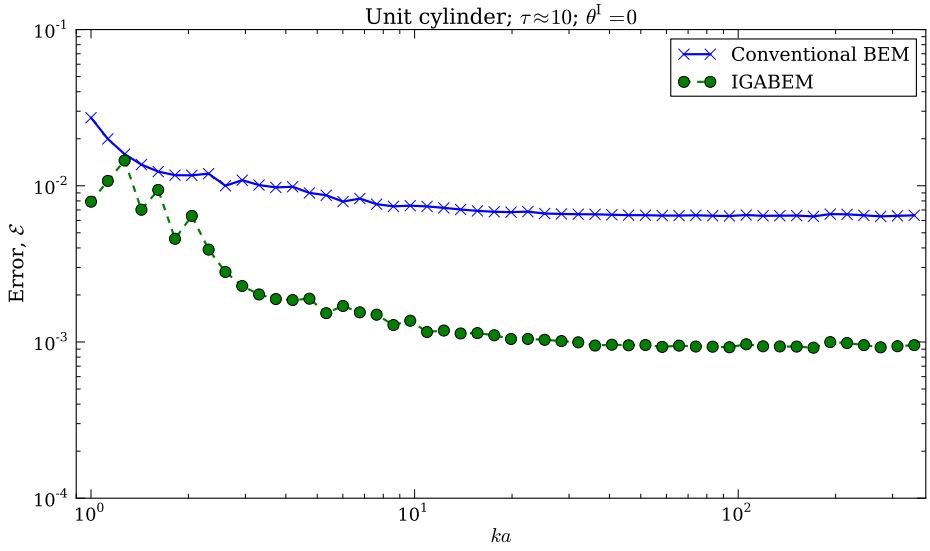

Figure 3: Comparison of accuracy of conventional BEM and IGABEM simulations for the hard cylinder problem.

To draw a comparison between XIBEM and IGABEM simulations, first a study of simulation accuracy with respect to the variable τ is conducted. For XIBEM simulations, the original mesh can be used with no knot refinement. Instead, the number of plane waves, M, in the expansion on each NURBS function can be varied; by including the same number of waves in each expansion, $\tau = M(J+1)/ka$. Fig. 4 shows the accuracy of IGABEM and XIBEM simulations of the cylinder problem for a fixed ka and varying τ.

The accuracy of IGABEM simulation increases with increasing τ; for $\sim 1\%$ accuracy, $\tau \approx 5$ is required. For lower values of τ, the accuracy of XIBEM simulations increases with an increasing τ and $\sim 1\%$ accuracy is obtainable for $\tau \approx 2.5$; however, for $\tau > 6$, the accuracy of the method appears to be at a maximum.

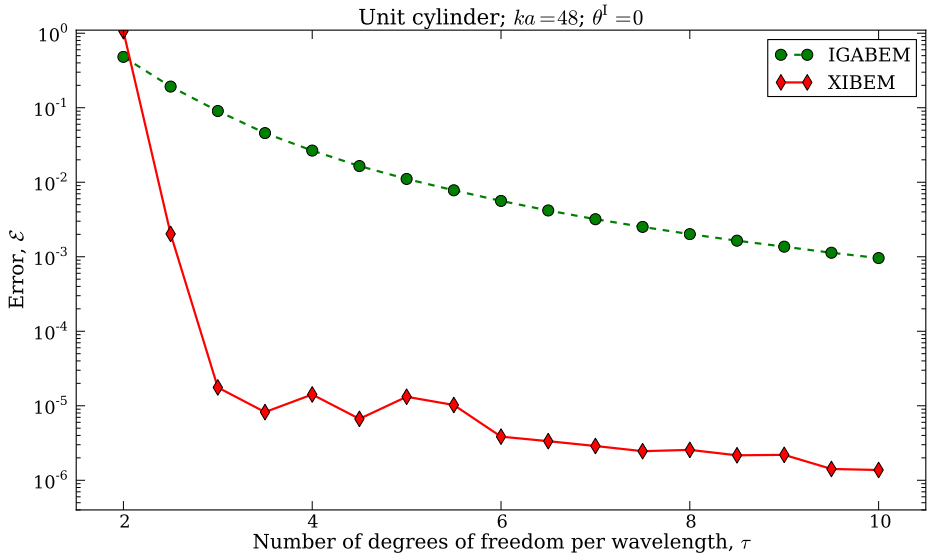

Figure 4: Comparison of accuracy of IGABEM and XIBEM simulations, for the hard cylinder problem, with respect to the number of degrees of freedom.

The cause of this plateau in accuracy can be explained by examining the condition number of the simulation matrices. The inclusion of the highly oscillatory plane waves in the XIBEM simulations deteriorates the conditioning of the system matrix. Fig. 5 shows the condition number of the simulations in Fig. 4. It appears that the condition number of the XIBEM system matrices also reaches a plateau for $\tau > 6$; however, it is observable that this maximum is approximately 10^{16} which is a computational limit of the SVD

routine used in this work. Conversely, the conditioning of the IGABEM simulations appears to be consistent and significantly better than that of the XIBEM simulations. PUM researchers of wave problems commonly report conditioning problems; however, as shown here, the use of a truncated SVD to solve the linear system handles the ill-conditioning well so that solutions of a high accuracy can be gained. As M becomes considerably larger than used in this study, the level of ill-conditioning could increase to a level at which SVD cannot obtain a reasonable solution. However, if J is increased and M decreased, the conditioning of the system can be controlled.

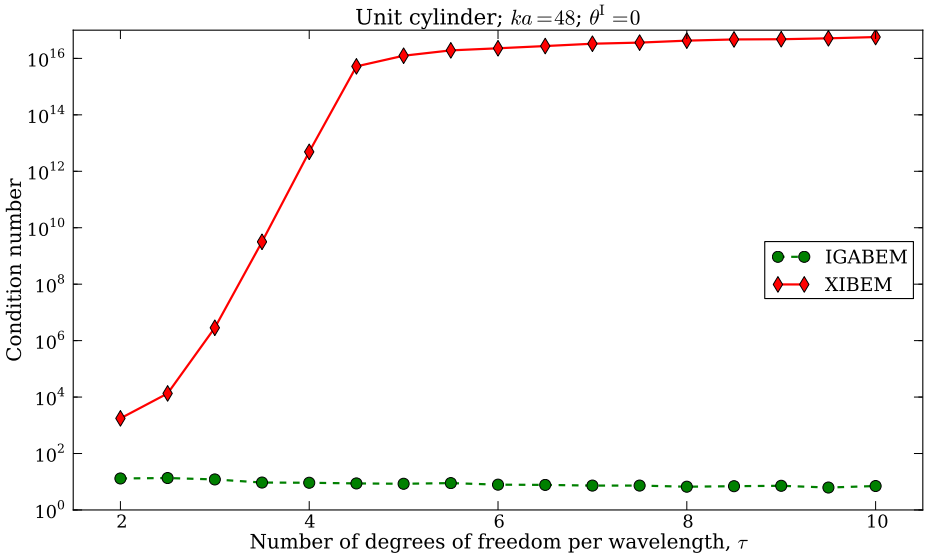

Figure 5: Comparison of system matrix condition numbers of IGABEM and XIBEM simulations, for the hard cylinder problem, with respect to the number of degrees of freedom.

A further comparison of IGABEM and XIBEM simulations is carried out for, now for varying ka. τ is now approximately fixed: $\tau \approx 10$ for IGABEM simulations; $\tau \approx 3$ for XIBEM simulations. The reader is reminded that this

means the XIBEM simulations are computed using only 30% of the number of degrees of freedom use in the IGABEM simulations. Fig. 6 shows the errors, $\mathcal{E}$, of the IGABEM and XIBEM simulation for $30 \leq ka \leq 500$. As ka increases, the error in the XIBEM approximations decreases rapidly reaching a minimum of approximately 10^{-6}. The IGABEM simulations provide a consistent approximation with an error of approximately 10^{-3}.

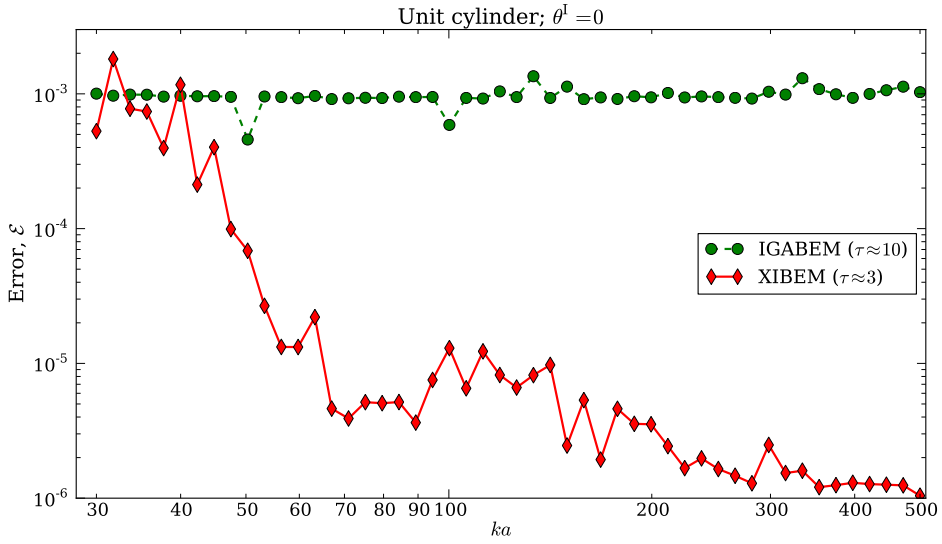

Figure 6: Comparison of accuracy of IGABEM and XIBEM simulations, for the hard cylinder problem, for fixed τ and varying ka.

Fig. 7 shows the condition numbers of the system matrices of the simulations in Fig. 6. As in the case of varying τ, the conditioning of the IGABEM system matrices is stable, with a condition number $< 10^2$. The increasing ka, and therefore increasing M, leads to degraded conditioning of the XIBEM system matrices. Again, they reach a computational maximum $\sim 10^{16}$; this point on the ka axis corresponds approximately with maximum

accuracy obtained in Fig. 6. In terms of the reduction of errors, the system solver routine appears to be the limiting factor of the XIBEM simulations; however, SVD is clearly still capable of recovering approximations with an error of $\sim 10^{-6}$ even when the system is very poorly conditioned.

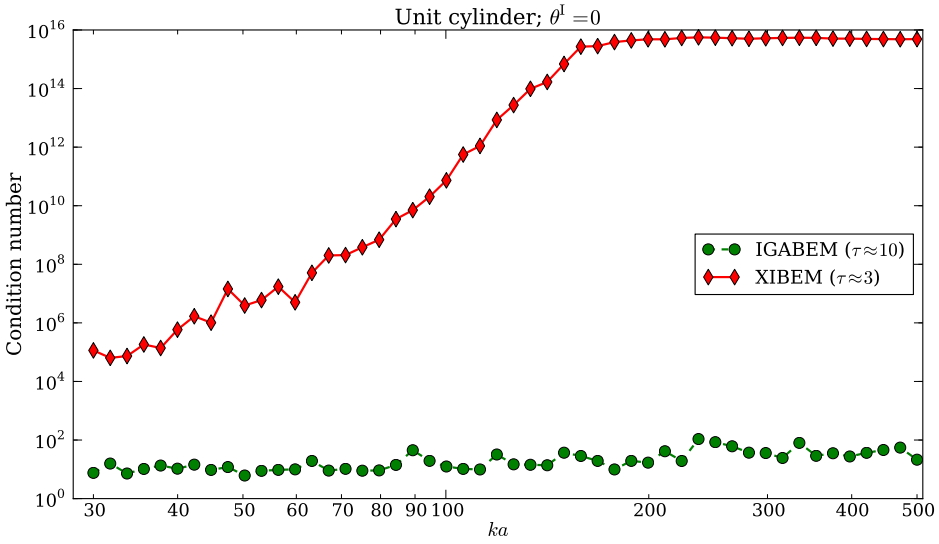

Figure 7: Comparison of system matrix condition numbers of IGABEM and XIBEM simulations, for the hard cylinder problem, for fixed τ and varying ka.

Finally, the XIBEM is compared to the partition-of-unity enriched PU-BEM. PU-BEM simulations are run using continuous quadratic elements and also using trigonometric elements as presented in [32]. The errors, $\mathcal{E}$, of the the XIBEM and PU-BEM simulations can be seen in Fig. 8. The accuracy of the simulations over the range of ka studied are similar. No method can be said to be significantly more accurate than another. It should be noted, however, that the PU-BEM simulations do not use the quadratic or trigonometric shape functions to locate integration or collocation points. These

points are carefully placed on the analytical surface of the scatterer; failure to do so results in unsuccessful simulations with errors $> 100\%$. Therefore, the XIBEM simulations hold a significant advantage over the PU-BEM in that the integration and collocation points are automatically mapped to the analytical surface.

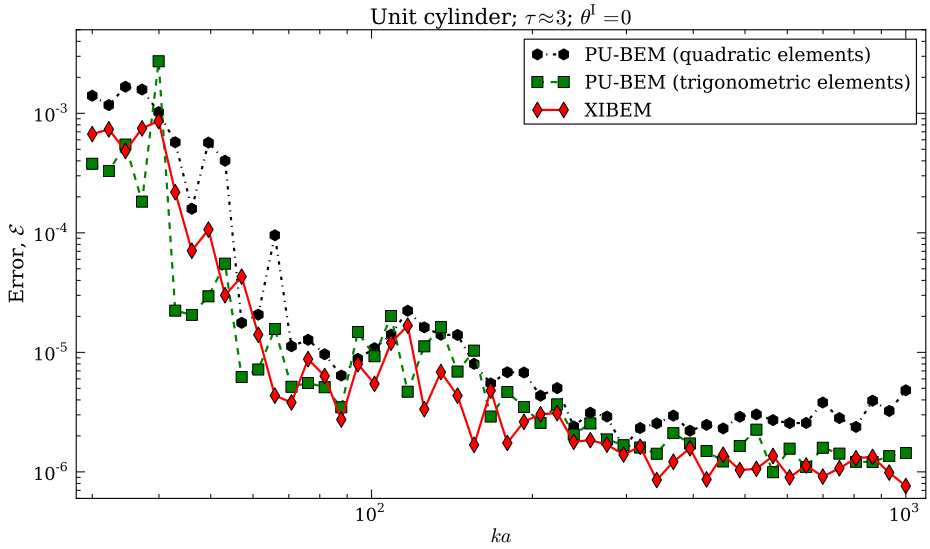

Figure 8: Comparison of accuracy of XIBEM and PU-BEM simulations, for the hard cylinder problem, for fixed $\tau \approx 3$ and varying ka.

4.2. Multiple scatterers

A second numerical example is included to demonstrate the ability of these boundary element simulations to approximate solutions to problems of multiple scatterers and with internal reflections. The geometry includes a unit-cylinder as described in Section 4.1, but now centred at (2,0). A capsule is defined as two semi-circular arcs centred at (1,0) and (-1,0) and

rotating through $\pi/2 > \theta > -\pi/2$ and $3\pi/2 > \theta > \pi/2$ respectively; these arcs are joined by straight line segments of length 2. The geometry includes two of these capsules, rotated $\pm\pi/4$ and translated through (-1,2) and (-1,-2) respectively. Fig. 9 displays the multi-scatterer geometry and illustrates the absolute value of the total potential, with an incident wave propagating at incidence angle $\theta^{\mathrm{I}} = 3\pi/4$. No analytical solution for this problem is available; instead, a converged solution using the method of fundamental solutions (MFS) [33] is used as a reference solution when calculating the errors, $\mathcal{E}$.

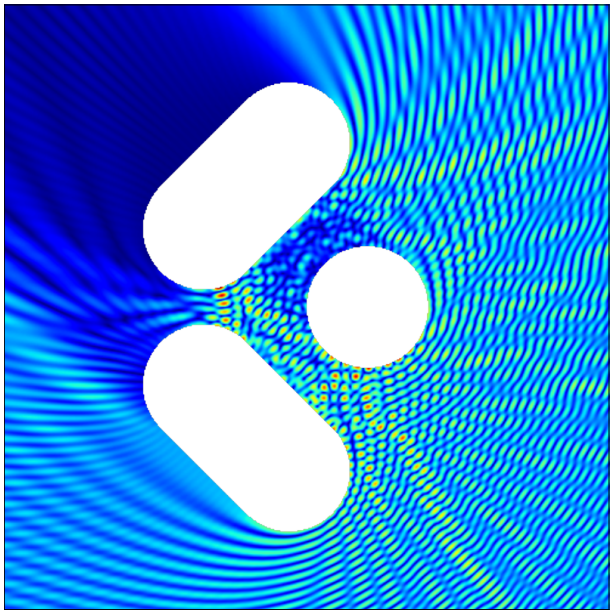

Figure 9: A plot of $\|\phi\|$ illustrating of the internal reflections and scattering caused by the multi-scatterer geometry: $ka = 25$, $\theta^{\mathrm{I}} = 3\pi/4$.

Figure 10 displays the errors in conventional BEM, IGABEM and XIBEM simulations of the multi-scatterer problem. For each simulation type, the number of degrees of freedom per wavelength, τ, is noted in the figure legend;

it can be seen that XIBEM are results are obtained using three times fewer degrees of freedom than used by the other simulations. The IGABEM approximations are clearly more accurate than those of the conventional BEM; furthermore, the XIBEM approximations have smaller errors than both.

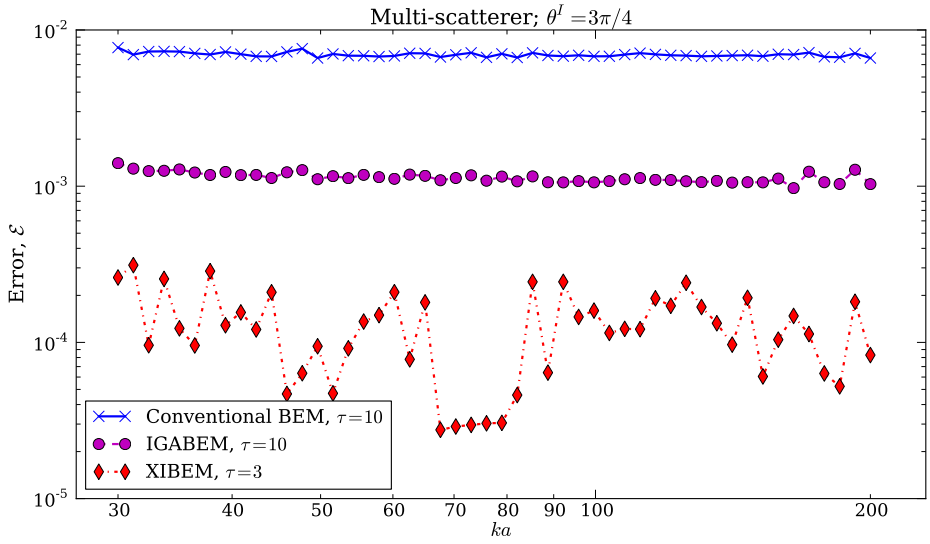

Figure 10: Comparison of accuracy of conventional BEM, IGABEM and XIBEM simulations, for the multi-scatterer problem, for fixed τ and varying ka.

For this problem, condition numbers for conventional BEM simulations and IGABEM simulations are similar, in the range 28–215. These are well conditioned in comparison with XIBEM simulations which have a consistent condition number $\sim 10^{16}$. Unlike the case of the single cylinder problem, the XIBEM system matrices are ill-conditioned for lower values, as well as higher values, of ka. This is because the number of plane waves, M, in the expansion on each NURBS function varies between the cylinder and capsule scatterers. Regardless of the ill-conditioned system matrices of the XIBEM

simulations, the SVD of these can provide approximations more accurate than the IGABEM by over an order of magnitude.

Finally, Fig. 11 compares the accuracy of XIBEM simulations with PU-BEM simulations. With the exception of problems for $ka < 20$, the accuracy of XIBEM and PU-BEM simulations are indistinguishable in this form; nor does the examination of the numerical values provide any significant indication that one method provides consistently more accurate solutions than another. Nearly all of the increased accuracy of this method is found in the plane wave expansion; these findings are the same similar to those found in [32]. It should be noted again, however, that the collocation and integration points have to be placed on the analytical surface of the scatterer which is inherent in the XIBEM formulation but requires prudence with the PU-BEM formulation.

4.3. Run time

The recursive nature of the NURBS functions makes them more computationally expensive to compute than Lagrangian functions; however, efficient algorithms [20] can reduce this overhead. This work has made use of Bézier decomposition, in which the NURBS curve is decomposed into Bézier elements for which the basis functions are less computationally expensive to compute. An alternative method, Bézier extraction [34], exploits this relationship between NURBS and Bézier curves without the need to explicitly decompose the original curve.

The evaluation of the highly oscillatory plane waves in the XIBEM enrichment is also more expensive than evaluating a basis with only nodal values of potential and shape functions; however, this computational expense comes

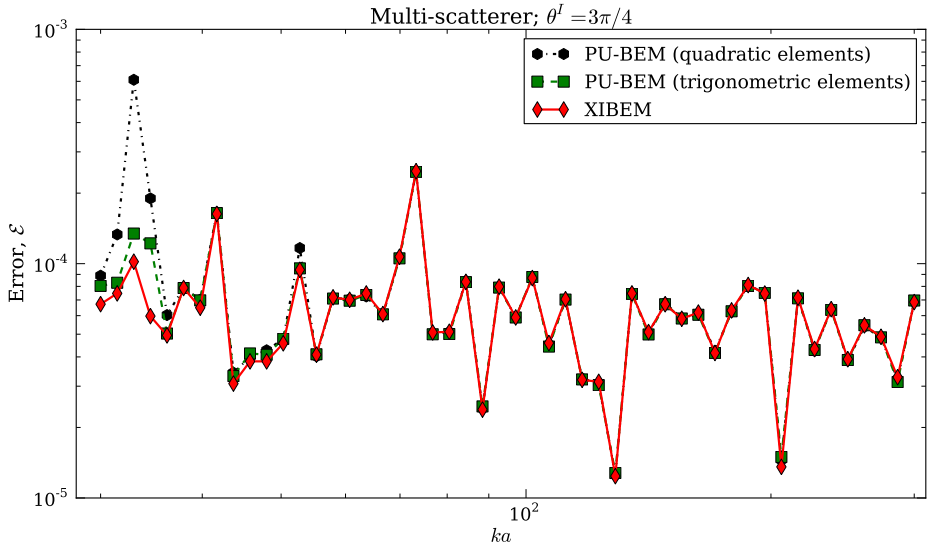

Figure 11: Comparison of accuracy of XIBEM and PU-BEM simulations, for the multi-scatterer problem, for fixed $\tau = 3$ and varying ka.

with the benefit of significantly smaller system matrices, reducing system building and solving times. Normalised run times for some approximations by the conventional BEM, IGABEM and XIBEM can be seen in Table 1. Simulations were run using Python and the times are used only as an indicator; doubtless, more efficient implementations of all three methods are possible.

Efficient quadrature for isogeometric analysis is a current topic of research [35]. However, in this work, no special integration schemes were used for any of the approaches. For conventional BEM simulations, six-point quadrature was used to integrate over each element. For IGABEM simulations, six-point quadrature was used to integrate over each knot span. For XIBEM simulations, each knot span was considered as a set of integration cells of

Table 1: Comparison of simulation times for multi-scatterer problem

	Degrees of freedom	System build (s/467.89)	System solve (s/978.50)	L_2 error $\mathcal{E}$
$ka = 30$, BEM	1600	0.0128	0.0076	7.7×10^{-3}
$ka = 30$, IGABEM	1600	0.0417	0.0128	1.4×10^{-3}
$ka = 30$, XIBEM	480	0.0046	0.0008	2.6×10^{-4}
$ka = 70$, BEM	3580	0.0637	0.0902	6.9×10^{-3}
$ka = 70$, IGABEM	3580	0.1622	0.1467	1.1×10^{-3}
$ka = 70$, XIBEM	1075	0.0200	0.0198	2.9×10^{-5}
$ka = 150$, BEM	7600	0.5719	0.8364	6.8×10^{-3}
$ka = 150$, IGABEM	7600	1.0000	1.0000	1.1×10^{-3}
$ka = 150$, XIBEM	2280	0.0854	0.0907	6.1×10^{-5}

length $\pi/4$; each cell was then integrated using six-point quadrature.

It can be seen that the improved accuracy of the IGABEM simulations comes at the expense of more computationally expensive basis functions. The system matrices can take more than twice as long to evaluate than the conventional BEM. The solving of system matrices also takes longer for the IGABEM. The XIBEM simulations take considerably less time to run. This is expected as the system matrices contain eleven-times fewer entries than those of the conventional BEM and IGABEM simulations; however, the more complicated integration of the XIBEM basis functions reduces this time saving during the system build stage of the simulations. Overall, it is clear that XIBEM simulations take less time than both conventional BEM and IGABEM simulations, while providing more accurate solutions.

5. Conclusions

This paper has presented two formulations of isogeometric boundary element methods for two-dimensional Helmholtz problems.

In the first formulation, the IGABEM, the geometries of a problem and the approximation of the potential function over the boundary of acoustic scatterers are described by NURBS functions. The analytical geometry, provided by NURBS functions, used in the integration of the boundary integrals, and the NURBS-approximated function on the scatterer boundary, lead to reduced errors compared to a conventional BEM scheme.

In the second formulation, the XIBEM, the IGABEM has been extended by the use of a plane wave basis to express the wave potential. The superior accuracy of this approach has been demonstrated for problems of single and multiple scatterers with smooth boundaries. These superior accuracies are achieved despite a significant reduction in the degrees of freedom required for a given problem; for an accuracy of $\sim 1\%$, three-times fewer degrees of freedom are required for XIBEM simulations than for conventional BEM or IGABEM simulations. This reduction in system size means that simulations take less time and, for a fixed computational memory resource, problems of shorter wavelengths are possible. This extends the effective bandwidth for which the isogeometric boundary element approach is valid.

Though small, the system matrices from XIBEM simulations are generally ill-conditioned. It has been shown that singular value decomposition is an effective solver for these type of matrices; indeed, the authors found no limit to the scheme other than the available computer memory.

Errors for XIBEM and PU-BEM were compared and found to be sim-

ilar. However, empirically it has been found there is a requirement, with the partition-of-unity enrichment, for collocation and integration points to be placed on the analytical surface of a scatterer. For PU-BEM simulations, this creates significant difficulties for more complex geometries as these points cannot be recovered from the Lagrangian shape functions. The NURBS functions used in XIBEM simulations provide the analytical geometry inherently and, thus, any geometry from CAD software can be analysed with little or no need for meshing. This is a significant benefit of the XIBEM over PU-BEM simulations.

It is expected that the small system matrices of XIBEM will be of greater benefit in three-dimensional problems where it may be possible to use approximately 40-times fewer degrees of freedom than the conventional BEM. However, three-dimensional problems present new challenges. For example, finding and choosing equally-spaced plane wave directions for the enrichment is more complex than the two-dimensional case. Methods do exist, though no study of the efficacy of the approaches has been carried out. The integration of the singular integrals near collocation points requires special schemes. Though regularisation methods can make this easier, the placement of collocation points may have a considerable impact. The inclusion of the plane wave enrichment will have a significant impact on the conditioning of the system. However, in PU-BEM research, the conditioning of system matrices has found to be better in three-dimensional than in two-dimensional problems; this means that more efficient solving algorithms such as QR decomposition can be used instead of SVD [36].

References

[1] T. J. R. Hughes, J. A. Cottrell, Y. Bazilevs, Isogeometric analysis: CAD, finite elements, NURBS, exact geometry and mesh refinement, Computer Methods in Applied Mechanics and Engineering 194 (2005) 4135 – 4195.

[2] Y. Bazilevs, V. M. Calo, J. A. Cottrell, J. A. Evans, T. J. R. Hughes, S. Lipton, M. A. Scott, T. W. Sederberg, Isogeometric analysis using T-splines, Computer Methods in Applied Mechanics and Engineering 199 (2010) 229 – 263.

[3] J. A. Cottrell, A. Reali, Y. Bazilevs, T. J. R. Hughes, Isogeometric analysis of structural vibrations, Computer Methods in Applied Mechanics and Engineering 195 (2006) 5257 – 5296.

[4] Y. Bazilevs, V. M. Calo, T. J. R. Hughes, Y. Zhang, Isogeometric fluid-structure interaction: theory, algorithms, and computations, Computational Mechanics 43 (2008) 3–37.

[5] A. Buffa, G. Sangalli, R. Vázquez, Isogeometric analysis in electromagnetics: B-splines approximation, Computer Methods in Applied Mechanics and Engineering 199 (2010) 1143 – 1152.

[6] E. De Luycker, D. J. Benson, T. Belytschko, Y. Bazilevs, M. C. Hsu, X-FEM in isogeometric analysis for linear fracture mechanics, International Journal for Numerical Methods in Engineering 87 (2011) 541–565.

[7] R. N. Simpson, S. P. A. Bordas, J. Trevelyan, T. Rabczuk, A two-dimensional isogeometric boundary element method for elastostatic

analysis, Computer Methods in Applied Mechanics and Engineering 209-212 (2012) 87 – 100.

[8] C. Politis, A. I. Ginnis, P. D. Kaklis, K. Belibassakis, C. Feurer, An isogeometric BEM for exterior potential-flow problems in the plane, in: 2009 SIAM/ACM Joint Conference on Geometric and Physical Modeling, SPM '09, ACM, New York, NY, USA, 2009, pp. 349–354.

[9] T. Takahashi, T. Matsumoto, An application of fast multipole method to isogeometric boundary element method for Laplace equation in two dimensions, Engineering Analysis with Boundary Elements 36 (2012) 1766 – 1775.

[10] M. A. Scott, R. N. Simpson, J. A. Evans, S. Lipton, S. P. A. Bordas, T. J. R. Hughes, T. W. Sederberg, Isogeometric boundary element analysis using unstructured T-splines, Computer Methods in Applied Mechanics and Engineering 254 (2013) 197–221.

[11] T. Abboud, J. C. Nédélec, B. Zhou, Improvement of the integral equation method for high frequency problems, in: Third International Conference on Mathematical and Numerical Aspects of Wave Propagation, SIAM Proceedings Series, SIAM, Philadelphia, 1995, pp. 178–187.

[12] O. P. Bruno, C. A. Geuzaine, J. A. Monro, F. Reitich, Prescribed error tolerances within fixed computational times for scattering problems of arbitrarily high frequency: the convex case, Philosophical Transactions of the Royal Society of London. Series A: Mathematical, Physical & Engineering Sciences 362 (2004) 629–645.

[13] S. Langdon, S. N. Chandler-Wilde, A wavenumber independent boundary element method for an acoustic scattering problem, SIAM Journal of Numerical Analysis 43 (2006) 2450–2477.

[14] V. Domínguez, I. G. Graham, V. P. Smyshlyaev, A hybrid numerical-asymptotic boundary integral method for high-frequency acoustic scattering, Numerische Mathematik 106 (2007) 471–510.

[15] A. Anand, Y. Boubendir, F. Ecevit, F. Reitich, Analysis of multiple scattering iterations for high-frequency scattering problems. II: The three-dimensional scalar case, Numerische Mathematik 114 (2009) 373–427.

[16] J. M. Melenk, I. Babuška, The partition of unity finite element method: Basic theory and applications, Computer Methods in Applied Mechanics and Engineering 139 (1996) 289 – 314.

[17] A. de la Bourdonnaye, A microlocal discretization method and its utilization for a scattering problem, Comptes Rendus de l'Académie des Sciences - Série I 318 (1994) 385–388.

[18] H. Bériot, E. Perrey-Debain, M. B. Tahar, C. Vayssade, Plane wave basis in Galerkin BEM for bidimensional wave scattering, Engineering Analysis with Boundary Elements 34 (2010) 130–143.

[19] E. Perrey-Debain, J. Trevelyan, P. Bettess, Plane wave interpolation in direct collocation boundary element method for radiation and wave scattering: numerical aspects and applications, Journal of Sound and Vibration 261 (2003) 839–858.

[20] L. Piegl, W. Tiller, The NURBS book, Springer-Verlag, 2nd edition, 1997.

[21] L. C. Wrobel, The boundary element method: applications in thermo-fluids and acoustics, volume 1, John Wiley & Sons, 2002.

[22] A. A. Becker, The boundary element method in engineering: a complete course, McGraw-Hill, Maidenhead, 1992.

[23] J. C. F. Telles, A self-adaptive co-ordinate transformation for efficient numerical evaluation of general boundary element intergrals, International Journal for Numerical Methods in Engineering 24 (1987) 959–973.

[24] J. C. F. Telles, R. F. Oliveira, Third degree polynomial transformation for boundary element integrals: further improvements, Engineering Analysis with Boundary Elements 13 (1994) 135–141.

[25] T. Greville, Numerical procedures for interpolation by spline functions, Journal of the Society for Industrial and Applied Mathematics Series B Numerical Analysis 1 (1964) 53–68.

[26] R. W. Johnson, Higher order B-spline collocation at the Greville abscissae, Applied Numerical Mathematics 52 (2005) 63 – 75.

[27] T. Kim, V. Dominguez, I. G. Graham, V. P. Smyshlyaev, Recent progress on hybrid numerical-asymptotic method for high-frequency scattering problems, in: 7th UK Conference on Boundary Integral Methods (UKBIM7), Nottingham.

[28] S. N. Chandler-Wilde, I. G. Graham, S. Langdon, E. A. Spence, Numerical-asymptotic boundary integral methods in high-frequency scattering, Acta Numerica 21 (2012) 89–305.

[29] M. E. Honnor, J. Trevelyan, D. Huybrechs, Numerical evaluation of the two-dimensional partition of unity boundary integrals for Helmholtz problems, Journal of Computational and Applied Mathematics 234 (2010) 1656–1662.

[30] H. A. Schenck, Improved integral formulation for acoustic radiation problems, Journal of the Acoustical Society of America 44 (1968) 41–58.

[31] D. S. Jones, Acoustic and electromagnetic waves, Clarendon Press, Oxford, 1986.

[32] M. J. Peake, J. Trevelyan, G. Coates, Novel basis functions for the partition of unity boundary element method for Helmholtz problems, International Journal for Numerical Methods in Engineering 93 (2012) 905–918.

[33] P. S. Kondapalli, D. J. Shippy, G. Fairweather, Analysis of acoustic scattering in fluids and solids by the method of fundamental solutions, Journal of the Acoustical Society of America 91 (1992) 1844–1854.

[34] M. J. Borden, M. A. Scott, J. A. Evans, T. J. R. Hughes, Isogeometric finite element data structures based on Bézier extraction of NURBS, International Journal for Numerical Methods in Engineering 87 (2011) 15–47.

[35] T. J. R. Hughes, A. Reali, G. Sangalli, Efficient quadrature for NURBS-based isogeometric analysis, Computer Methods in Applied Mechanics and Engineering 199 (2010) 301 – 313.

[36] E. Perrey-Debain, O. Laghrouche, P. Bettess, J. Trevelyan, Plane-wave basis finite elements and boundary elements for three-dimensional wave scattering, Philosophical Transactions of the Royal Society of London. Series A: Mathematical, Physical & Engineering Sciences 362 (2004) 561–577.